

# An Investigation of the Ranges of Validity of Asteroid Thermal Models for Near-Earth Asteroid Observations

M. Mommert<sup>1</sup>

R. Jedicke<sup>2</sup>

D. E. Trilling<sup>1</sup>

## ABSTRACT

The majority of known asteroid diameters are derived from thermal infrared observations. Diameters are derived using asteroid thermal models that approximate their surface temperature distributions and compare the measured thermal infrared flux with model-dependent predictions. The most commonly used thermal model is the Near-Earth Asteroid Thermal Model (NEATM, Harris 1998), which is usually perceived superior to other models like the Fast-Rotating Model (FRM, Lebofsky & Spencer 1989). We investigate the applicability of the NEATM and the FRM to thermal-infrared observations of Near-Earth Objects using synthetic asteroids with properties based on the real Near-Earth Asteroid (NEA) population. We find the NEATM to provide more accurate diameters and albedos than the FRM in most cases, with a few exceptions. The modeling results are barely affected by the physical properties of the objects, but we find a large impact of the solar phase angle on the modeling results. We conclude that the NEATM provides statistically more robust diameter estimates for NEAs observed at solar phase angles less than  $\sim 65^\circ$ , while the FRM provides more robust diameter estimates for solar phase angles greater than  $\sim 65^\circ$ . We estimate that  $<5\%$  of all NEA diameters and albedos derived up to date are affected by systematic effects that are of the same order of magnitude as the typical thermal model uncertainties. We provide statistical correction functions for diameters and albedos derived using the NEATM and FRM as a function of solar phase angle.

*Subject headings:* Minor planets, asteroids

---

<sup>1</sup>Department of Physics and Astronomy, Northern Arizona University, Flagstaff, AZ 86011, USA

<sup>2</sup>Institute for Astronomy, University of Hawai'i at Manoa, Honolulu, HI 96822, USA

## 1. Introduction

Within the last decade, thermal-infrared observations and thermal modeling of asteroids have increased the number of asteroids with measured diameters and albedos by orders of magnitude. This increase can be mostly attributed to a new generation of space-based infrared telescopes that have been utilized in a number of asteroid discovery and characterization surveys: the *Spitzer Space Telescope* (Werner et al. 2004) has been used in the ExploreNEOs (Trilling et al. 2010), NEOSurvey (Trilling et al. 2016), and ongoing NEOLegacy characterization surveys, among many other asteroid-related observations; *Akari* (Usui et al. 2011) all-sky observations have been used to establish the “Asteroid catalog using Akari”; and the *Wide-field Infrared Survey Explorer* (WISE, Wright et al. 2010) has been used in the NEOWISE program (Mainzer et al. 2011b) in an all-sky discovery and characterization survey. More than 100,000 main belt asteroids and about 2,500 near-Earth asteroids (NEAs) with perihelion distances  $q \leq 1.3$  au have measured diameters and albedos using this method (also see Mainzer et al. 2015, for a discussion).

The majority of asteroid thermal data is interpreted using radiometric or thermal models. Asteroid thermal models combine thermal-infrared and optical brightness measurements in a simplified representation of the asteroid’s surface temperature distribution that allows for a derivation of the asteroid’s diameter and albedo. The most widely used thermal model is the Near-Earth Asteroid Thermal Model (NEATM, Harris 1998). The NEATM is based on the earlier Standard Thermal Model (STM, e.g., Morrison & Lebofsky 1979), both of which assume a spherical shape of the model asteroid, a spin axis orientation perpendicular to the orbital plane, a very slowly rotating asteroid, and a Lambertian surface with a negligible thermal inertia. The resulting temperature distribution (see Figure 1, top) consists of concentric small circles of the same temperature centered on the sub-solar point; both models assume zero night-side thermal emission. The NEATM fully accounts for the solar phase angle of the observations, whereas the STM assumes the target to be observed at zero phase angle (STM and NEATM are identical in the zero phase angle case); an empirical phase correction for thermal-infrared fluxes was derived for the STM by Lebofsky & Spencer (1989) to compensate for this simplification. The NEATM also allows for a modulation of the surface temperature distribution with a variable beaming parameter  $\eta$ ; a fixed value of  $\eta$  was introduced in the “refined STM” from observations by Lebofsky et al. (1986). The beaming parameter accounts for thermal effects caused by a non-zero thermal inertia of the surface material, surface roughness, and the spin state of the real asteroid in a zero-th order approximation. The NEATM has been found to provide robust diameter and albedo estimates (Delbo’ 2004; Wright 2007; Harris et al. 2011; Mainzer et al. 2011a) and is usually preferred over the STM due to its flexibility. Harris et al. (2011) find NEATM diameters and albedos to be accurate within 20% and 50%, respectively.

A different thermal model that deviates from the definition of the NEATM in assuming a rapid rotation of the model asteroid and a very high thermal inertia of the surface material is the Fast-Rotating Model (FRM, Lebofsky & Spencer 1989). As a result of the body’s fast rotation, insolation is evenly distributed over the sphere and the resulting surface temperature distribution is iso-latitudinal; the equator is hottest and the temperature decreases towards the poles of the model asteroid (see Figure 1, center).

STM/NEATM and FRM represent two extreme cases: STM/NEATM assume no (or very slow) rotation and zero (or a very small) thermal inertia, whereas the FRM assumes a fast rotation and high thermal inertia. For the majority of asteroids, the NEATM performs significantly better than the FRM (Delbo’ 2004), which is due to its increased flexibility through the variable beaming parameter  $\eta$ , as well as the extreme assumptions characterizing the FRM. Generally, high thermal inertias and/or rotation rates are necessary to generate a surface temperature distribution similar to that of the FRM. However, Delbo’ (2004) found that the FRM produces more accurate diameter results than the NEATM for large phase angles.

Thermal modeling of NEAs technically does not differ from the modeling of any other type of atmosphereless body. However, there are some aspects of the properties of NEAs that should be taken into account to properly interpret their thermal modeling results. NEAs are closer to the Earth than other Solar System bodies. Hence, they can be observed at larger solar phase angles (the angle between the Sun and the observer as measured from the asteroid.) While the NEATM geometrically accounts for the solar phase angle, the zero night-side temperature assumed by the NEATM compromises diameter and albedo measurements with increasing solar phase angle (e.g., Delbo’ 2004; Wright 2007; Wolters & Green 2009). In some extreme cases – for instance fast rotation or high thermal inertia – the observed temperature distribution might be better represented by the FRM than the NEATM. Such scenarios are relevant since NEAs tend to have shorter rotational periods than larger and more distant asteroids (see rotational periods compiled by Warner et al. 2009). The current record-holder for the fastest-spinning asteroid, 2014 RC, completes one rotation in only 16 s (Moskovitz et al. 2015). As a result of their fast rotation, the FRM might provide more realistic diameters and albedos than the NEATM for these objects. This is especially relevant for the smallest NEAs to be discovered in the future, among which will be temporarily captured Earth satellites or minimoons (Granvik et al. 2012; Bolin et al. 2014) that come extremely close to Earth.

Previous studies investigating the accuracy of the NEATM applied to observations of NEAs have been conducted. Delbo’ (2004) and Wright (2007) utilized a comparison of the NEATM with asteroid thermophysical models to investigate the effects of solar phase

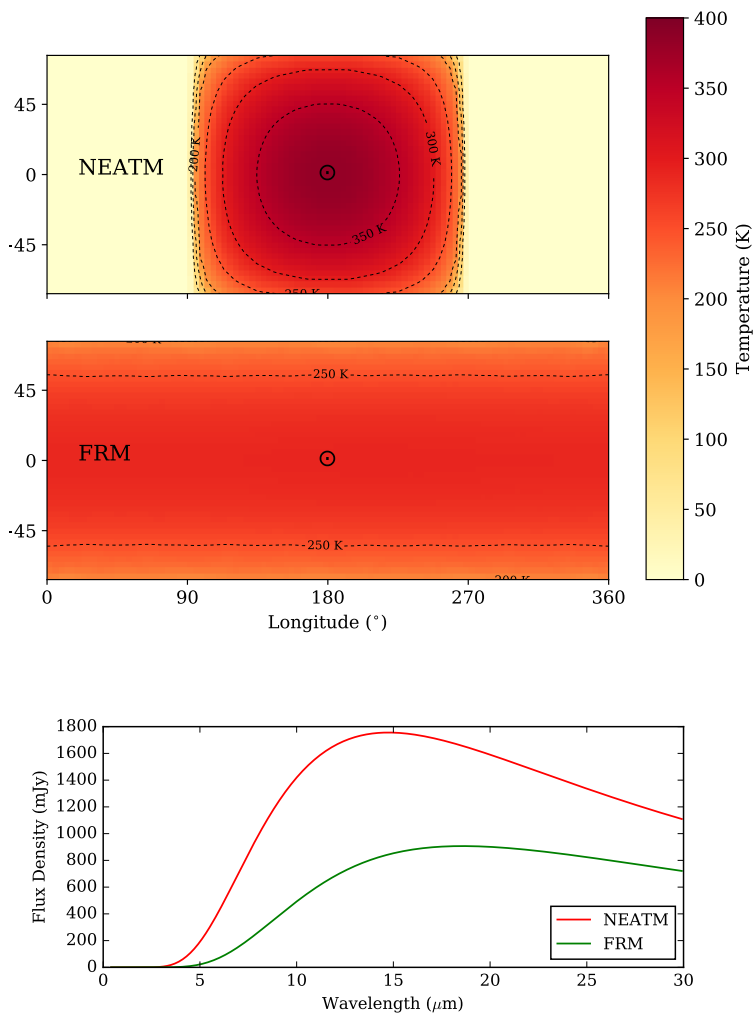


Fig. 1.— Representation of the surface temperature distributions assumed by the NEATM (top, using beaming parameter  $\eta = 1.0$ ) and FRM (center) for the same asteroid 1 au from the Sun. The subsolar point (Sun symbol) coincides with the sub-observer point in both plots. Contour lines refer to areas with similar temperatures. Note that the maximum temperature of the FRM is significantly lower than that of the NEATM. The bottom panel shows the spectral energy distribution (SED) caused by thermal emission for both models. The NEATM’s higher temperatures cause a shift of its SED peak towards shorter wavelengths as compared to the FRM.

angle, thermal inertia, and surface roughness on the NEATM accuracy. In this work, we elaborate on their approach and perform a more detailed and quantitative analysis of these effects on the modeled diameters and albedos as a function of asteroid physical properties and observation geometries. We consider conservative ranges for the physical properties based on our current picture of the NEA population and identify asteroid configurations under which the FRM is superior to the NEATM and provide a statistical analysis of the systematic effects on diameters and albedos derived with the NEATM and the FRM. The goal of this work is to provide a guideline for when thermal modeling results are reliable – or not – and how they should be interpreted.

The results of this work have important implications for the *a-priori* use of the NEATM in large-scale characterization programs and the thermal modeling of the smallest and closest NEAs.

## 2. Methodology

We explore the applicability of the NEATM and the FRM by simulating thermal-infrared flux densities for 1 million synthetic NEAs using an asteroid thermophysical model (TPM, Section 2.1) in a Monte Carlo approach. The physical properties and orbital geometries of these synthetic NEAs follow distributions that are typical for NEAs according to our best knowledge (Section 2.2). The simulated flux densities are modeled with NEATM and FRM implementations to derive diameter and albedo estimates (Section 2.3), which are subsequently compared against each other and the simulation input parameters (Section 2.4).

### 2.1. Simulated Flux Densities

We simulate thermal flux densities using a detailed asteroid thermophysical model. Thermophysical models (TPMs) allow for simulating the asteroid’s surface temperature distribution by solving the heat transfer equation numerically for a large number of plane surface facets. The TPM we use is mostly identical to, and has been tested extensively against, the one discussed by Mueller (2007) and has been used in other works, including Mommert et al. (2014a) and Mommert et al. (2014b). Our TPM implementation accounts for the spin axis orientation (longitude and latitude in ecliptic coordinates), rotational period, thermal inertia, and surface roughness in addition to observing geometry. TPMs can provide more accurate diameter and albedo estimates than simple thermal models, but they also require

additional constraints on the aforementioned parameters. In this work, we use the TPM to simulate flux densities for synthetic asteroids.

The TPM solves the heat transfer equation numerically for each surface facet until the sub-surface temperature at a certain depth varies less than a certain fractional threshold,  $\varepsilon_{\text{temp}}$  (usually  $\varepsilon_{\text{temp}} = 10^{-4}$ ), between two full rotations. For the sake of simplicity, we use a spherical shape for our model asteroids, each consisting of 496 triangular surface facets. Surface roughness is taken into account and modeled as emission from spherical craters using the approach taken by Mueller (2007); different models (no roughness, low roughness, default roughness, and high roughness) as defined in Mueller et al. (2004) are utilized here. In order to verify the conservation of energy in the model, the amount of incoming and outgoing energy are compared against each other. If there is an energy discrepancy of 1% or greater,  $\varepsilon_{\text{temp}}$  is reduced by an order of magnitude. This adjustment improves the conservation of energy and leads to more accurate flux densities – but also requires more computation time.

The wavelengths at which the flux densities are simulated sample the peaks of the asteroids’ spectral energy distributions well: 5–20  $\mu\text{m}$  at intervals of 5  $\mu\text{m}$ . Note that reflected solar light is not considered as part of this work. Flux density uncertainties, which are necessary for the proper interpretation of the flux densities as part of the  $\chi^2$  minimization in the thermal models (see Section 2.3), are assumed to follow a Poisson distribution and hence are the square-root of the derived flux at each wavelength (in order to mimic the noise properties of real observations).

## 2.2. Parameter Space

We create a synthetic representation of the NEA population consisting of 1 million objects sampling the parameters of our TPM (see Section 2.1). The ranges we consider for the physical properties are typical for NEAs and we weight them according to their measured or modeled distributions. Orbital parameters are chosen from the population of known NEAs, as detailed below.

In order to simulate flux densities, we have to assume diameters and geometric albedos for our synthetic NEAs. Geometric albedos ( $p_V$ ) are drawn from the albedo distribution by Wright et al. (2016) measured for the NEA population during the cryogenic part of the WISE mission. Since the surface temperature distribution of an asteroid is independent of its size, we assume a constant absolute magnitude  $H_V = 18$  mag ( $G = 0.15$ ) for all objects; the target diameter follows from  $H_V$  and the respective geometric albedo value.

We draw ecliptic spin axis latitudes from a second-order polynomial distribution fit-

ted to the obliquity distribution derived by Farnocchia et al. (2013) (their Figure 6); this distribution is in agreement with later findings (Tardioli et al. 2017). Spin axis longitudes are drawn from a uniform distribution spanning  $360^\circ$  as there is no preference for spin axis longitudes. Other parameters are also drawn from uniform distributions due to a lack of additional information on the underlying distributions. We sample thermal inertias in the range  $\Gamma \in [20, 2000]$  SI units ( $1 \text{ SI Unit} = 1 \text{ J m}^{-2} \text{ s}^{-0.5} \text{ K}^{-1}$ ), which is motivated by Mommert et al. (2014a) and the fact that little is known about the un-biased distribution of NEA thermal inertias. Rotational periods are uniformly sampled from the interval  $P \in [10 \text{ sec}, 100 \text{ hr}]$ ; this range is consistent with the range of reliably measured rotational periods of NEAs compiled by Warner et al. (2009). We note that the distribution of rotational periods of NEAs and other asteroids is strongly biased (e.g., Masiero et al. 2009). Hence, we deliberately use a uniform distribution of rotational periods in order to probe the impact of rotational periods over a wide range. Finally, we uniformly sample the discrete roughness models [low, default, and high roughness] (see Mueller 2007, for definitions of these models); we consider the absence of surface roughness unrealistic for this study. We refer to Section 4 for a discussion of the range definitions and their implications.

In order to properly sample observation geometry, we use heliocentric and geocentric coordinates of 5,000 randomly selected real NEAs for a random epoch. All selected NEAs have solar elongation angles  $60 \leq \varepsilon \leq 180^\circ$ , restricting the sample to objects that are observable from the Earth and from space-based platforms with state-of-the-art thermal infrared telescopes. Hence, our set of orbital geometry parameters provides a snapshot of the NEA population that is accessible for observations. We verified that this subset of the NEA population represents the overall population well in heliocentric and geocentric distances, solar phase angle, and as a function of time (using different epochs). This verification was performed using a two-sided Kolmogorov-Smirnov test that compares the full ensemble of observable NEAs at different epochs with our random sample; in no case was there a significant probability that our sample was drawn from a different population.

For each of the 5,000 NEA geometries, we create 200 randomized sets of physical properties, resulting in a total of 1 million synthetic NEAs considered in this study. We do not consider noise contributions to the sampled parameters in order to be able to better work out the effects at work.

### 2.3. Thermal Modeling

The simulated flux densities are modeled using well-tested versions of the NEATM and the FRM, following the implementation by Delbo’ and Harris (2002). For each synthetic

NEA, we use all four generated thermal flux densities and fit them simultaneously taking into account the observing geometry and flux density uncertainties. The best fit is derived using a  $\chi^2$  minimization of the residuals between “measured” (generated by the TPM) and thermal model flux densities, weighted by the “measured” flux density uncertainties. The use of realistic (Poissonian) “measured” flux density uncertainties is necessary to weight the “measured” flux densities at the different wavelengths correctly. Improper uncertainties will lead to distorted best-fit spectral energy distributions and hence systematic effects on the derived diameters and albedos. Using this approach, we fit diameters and beaming parameters (NEATM only) for each object – albedos follow through the combination with the assumed absolute magnitude of the object. We use the same Solar System absolute magnitude as a measure for optical brightness for all objects, which does not affect the conclusion of this work. We refer to Mommert (2013) for a detailed discussion of the model implementations.

## 2.4. Analysis

For each synthetic object we can identify whether the NEATM or the FRM provides the more accurate diameter or albedo result by comparing our solutions to the input parameters utilized in the derivation of the flux densities using the TPM (see Section 2.1). For instance, the diameter derived with the NEATM is considered more accurate if  $|d_{\text{NEATM}} - d| < |d_{\text{FRM}} - d|$ , where  $d$  is the input diameter,  $d_{\text{NEATM}}$  is the diameter derived by the NEATM, and  $d_{\text{FRM}}$  is the diameter derived by the FRM. In order to characterize the impact of one specific physical or orbital parameter on diameter and albedo estimates, we marginalize over the other parameters and derive distributions where the NEATM (or the FRM) is more accurate. The **success rate** is defined as the fraction of cases where the NEATM (or FRM) provides a better fit over a marginalized distribution. The marginalized distribution is derived from the complete synthetic object distribution by summation over the success rates for all but one parameter. Hence, the success rate distribution for this one parameter is fully retained, whereas information from the other parameters has been marginalized out. For instance, the NEATM diameter success rate with respect to thermal inertia describes the fraction of cases in which the NEATM derives a more accurate diameter than the FRM as a function of thermal inertia; in this case, the success rates for all parameters except that of the thermal inertia are summed over, retaining the success rate distribution with respect to this parameter. This fraction can be interpreted as the probability of the NEATM to be superior to the FRM as a function of thermal inertia for a random asteroid. Success rates for the diameter and the albedo should be identical; we provide both quantities for the sake of completeness and discuss exceptions from this rule.



In order to quantify the agreement of thermal model results with the actual synthetic asteroid diameters and albedos, we introduce a second diagnostic quantity. For each synthetic asteroid, we calculate the quantity  $(d_{\text{NEATM}} - d)/d$ , which is the fractional error of the NEATM-derived diameter ( $d_{\text{NEATM}}$ ) from the actual input diameter ( $d$ ); errors for the FRM and for the geometric albedo can be defined correspondingly. By marginalizing over one parameter we can define the **median fractional error** as a function of this parameter. The marginalization is done as described above. However, in this case the median is derived instead of the sum of the other parameters. The marginalization enables the identification of systematic effects that occur as a function of individual parameters. The variation in the fractional errors is captured by the  $1\sigma$  and  $3\sigma$  envelopes that include 68.3% and 99.7% of all synthetic objects around the median in each bin, respectively.

### 3. Results

The following sections investigate the accuracy of the NEATM and the FRM as a function of different synthetic object parameters using the tools defined in Section 2.4.

#### 3.1. Physical Properties

Figure 2 shows success rates and fractional errors for rotational period, thermal inertia, surface roughness, and geometric albedo. NEATM success rates are greater than 80% and the NEATM median fractional errors are zero within the  $1\sigma$  intervals for all parameters, whereas the FRM fractional errors are systematically and significantly offset. Conditions that resemble the assumptions of the FRM (high thermal inertia, short rotation periods) lead to slightly higher success rates and lower fractional errors for the FRM and vice-versa for the NEATM. However, this effect is not significant. Increasing degrees of surface roughness lead to increasing fractional errors for both the NEATM and the FRM, but with different signs. This is expected since both the NEATM and the FRM assume Lambertian surfaces that are perfectly smooth. Finally, diameters and geometric albedos derived with both models are unaffected by the input geometric albedos of the synthetic objects.

The physical properties have only minor effects on the applicability of the NEATM, which is superior to the FRM in the vast majority of cases.

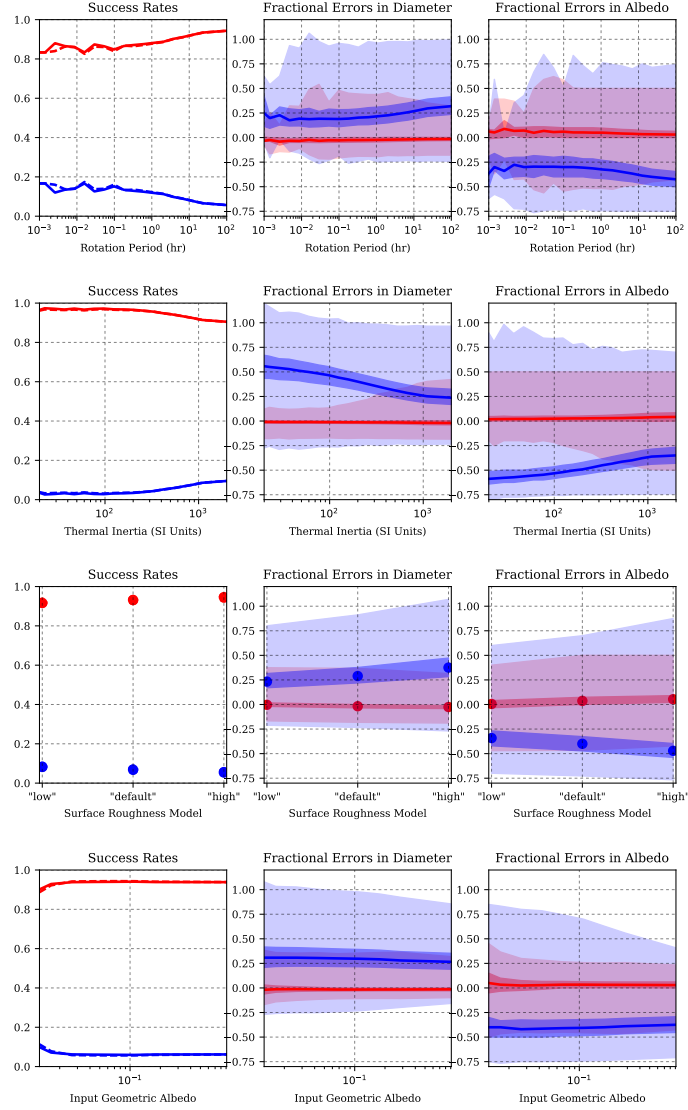


Fig. 2.— Success rates and fractional errors based on physical properties: rotation period (top row), thermal inertia (second from top), surface roughness (second from bottom), and geometric albedo (bottom row). In all plots, NEATM is indicated with red and FRM is indicated with blue. The left columns show NEATM and FRM success rates for diameter (solid line) and albedo (dashed line); the center column shows diameter median fractional errors (solid line) as well as its  $1\sigma$  (darker shading) and  $3\sigma$  (lighter shading) envelopes; the right column shows albedo fractional errors. For all properties considered here, the NEATM is more likely to provide accurate diameters and albedos than the FRM. NEATM median fractional errors are negligible, while FRM median fractional errors are significant.

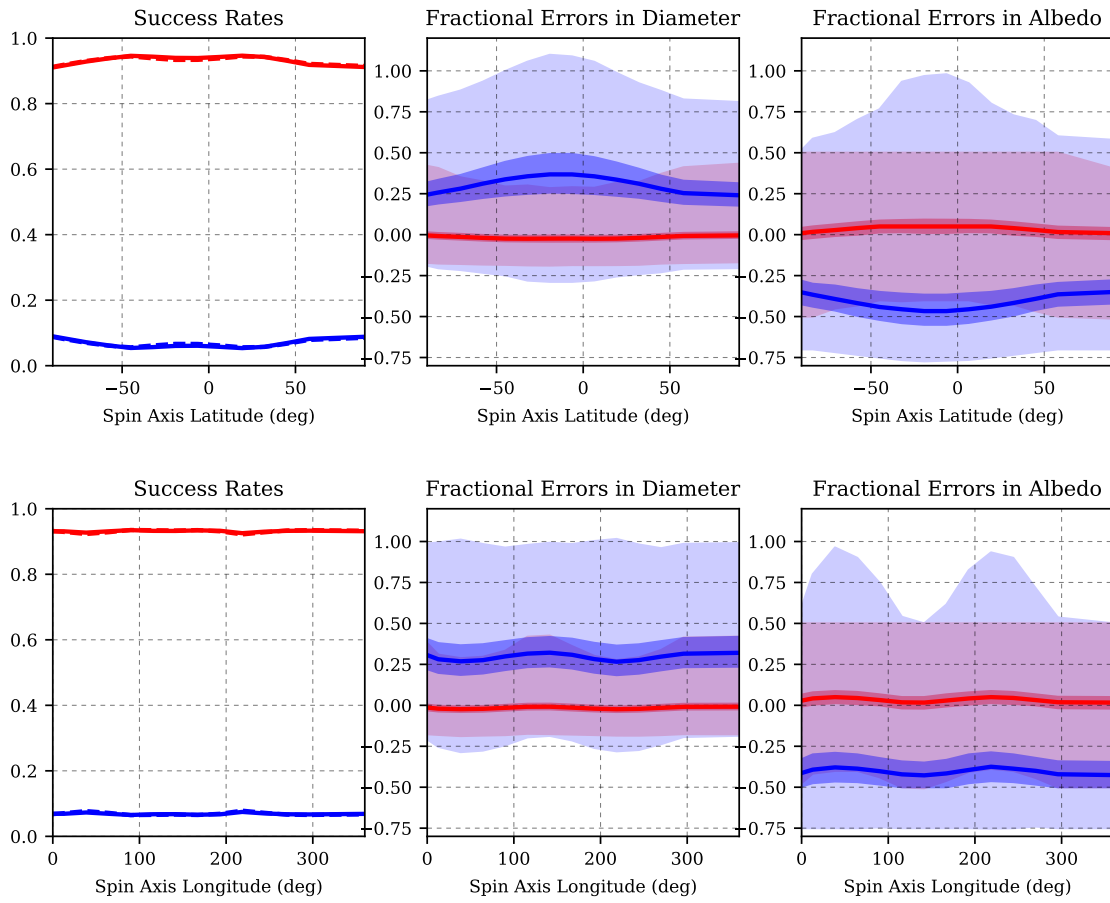


Fig. 3.— Success rates and fractional errors based on spin axis latitudes and longitudes. Refer to Figure 2 for definitions. Based on the success rates and fractional errors, the NEATM is more likely to provide accurate diameters and albedos than the FRM.

### 3.2. Spin Axis Orientation

The impact of the spin axis orientation on thermal modeling is shown in Figure 3. The NEATM success rates are greater 90% and NEATM fractional errors are negligible throughout the entire range in both parameters. While the fractional errors for the spin axis latitude show a dip/bump, the fractional errors for the spin axis longitude show a wavy pattern. The former effect, a dip in the fractional errors of the diameters (albedos) derived with the NEATM (FRM) and a bump in the fractional errors of the diameters (albedos) derived with the FRM (NEATM) at spin axis latitudes close to zero, is a result of the different surface temperature distributions assumed by the two thermal models that are more or less compatible with equator-on views. Similarly, the NEATM has higher success rates for spin axis latitudes around zero and the FRM has higher success rates for extreme spin axis latitudes ( $-90^\circ$  and  $+90^\circ$ ). At spin axis latitudes close to zero (and a random spin axis longitude), it is somewhat likely to have insolation and hence higher temperatures at the poles of the object, mimicking the NEATM surface temperature distribution and preferring the NEATM. In this case, the FRM overestimates diameters and underestimates albedos. At spin axis latitudes close to the extremes ( $-90^\circ$  and  $+90^\circ$ ), the largest fraction of the insolation falls near the equator, leading to a surface temperature distribution very similar to that of the FRM, penalizing the NEATM performance. The wavy pattern in the case of the spin axis longitude is caused by our selection effects for the orbital geometries: all geometries used in this simulation have the same epoch and solar elongations between  $60^\circ$  and  $180^\circ$  (see Section 2.2). For those synthetic objects with spin axis latitudes close to zero, the spin axis longitude decides whether insolation is focused on the poles or the equator. Hence, NEATM-preferred and FRM-preferred surface temperature distributions are spaced by  $90^\circ$  in spin axis longitude, causing a wave-like pattern in the fractional errors of this parameter.

Despite the complexity caused by the different spin axis configurations, the NEATM is more likely to provide accurate diameters and albedos for a random spin axis orientation of a random NEA.

### 3.3. Observing Geometry

We investigate the impact of the synthetic objects' observing geometry on the thermal modeling results. Since heliocentric distance, distance from the observer, and solar phase angle are closely related, we focus on the latter, which shows the effects most clearly (Figure 4). At solar phase angles up to  $65^\circ$ , the NEATM has a success rate close to unity and its fractional errors in diameter and albedo are close to zero. For phase angles greater than  $65^\circ$ , the FRM diameter success rate is greater than that of the NEATM. The situation is

more complicated for the albedo success rates of the NEATM and the FRM. This behavior is caused by the fact that the absolute diameter fractional errors of the NEATM grow faster than those of the FRM; FRM diameters are closer to the real diameters for solar phase angles greater  $65^\circ$ . On the other hand, the absolute albedo fractional errors of the NEATM grow slower than those of the FRM; for solar phase angles  $65^\circ \leq \alpha \leq 80^\circ$  the FRM derives on average slightly more accurate albedos than the NEATM, but for  $\alpha > 80^\circ$ , the NEATM performs slightly better again, causing the fluctuations in the albedo success rates.

The overall trend in the diameter and albedo fractional errors is a consequence of the oversimplified assumptions going into the thermal models. NEATM’s failing at phase angles greater than  $65^\circ$  is a result of its lack of night side emission. As the solar phase angle increases, a larger fraction of the asteroid’s night side, which is assumed to not contribute to its thermal emission, is observed. Observed flux densities are greater than modeled flux densities, leading to an overestimation of the object’s diameter. The fact that the FRM overestimates the diameter for solar phase angles less than  $65^\circ$  and underestimates it for greater phase angles stems from its limited capabilities to adapt more complex surface temperature distributions. At low solar phase angles, the observer sees the subsolar point, which is usually hotter than any temperature the FRM assumes, leading to an overestimation of the diameter. For high solar phase angles, the subsolar point is below the horizon and a large fraction of the night side is observed, underestimating the diameter. For both models, albedos are overestimated if diameters are underestimated and vice-versa.

### 3.4. Statistical Correction Functions

We take advantage of the systematic effect of the solar phase angle on the median fractional errors to establish statistical correction functions for diameter and albedo estimates derived with the NEATM and the FRM for individual objects. The correction functions are third-order polynomials that are fitted to the median fractional errors shown in Figure 5 (top panel) using a  $\chi^2$  minimization technique; the best-fit polynomial coefficients are listed in Table 1 and the fits are plotted in the top panel of Figure 5. The correction functions are of the form  $f(\alpha) = \sum_{i=0}^3 c_i \alpha^i$  with solar phase angle  $\alpha$  measured in degrees. In order to derive corrected diameters ( $d_{\text{corr}}$ ) from NEATM diameters ( $d_{\text{NEATM}}$ ), use the following relation:

$$d_{\text{corr}} = \frac{d_{\text{NEATM}}}{1 + f(\alpha)}, \quad (1)$$

where  $f(\alpha)$  is the corresponding NEATM diameter function and  $\alpha$  the solar phase angle in degrees. FRM and albedo corrections are performed correspondingly. The corrections can

be applied to individual objects. The limitations of this approach are discussed in Section 4.

The bottom panel of Figure 5 shows the median fractional errors for the NEATM and the FRM after the statistical corrections have been applied to each individual synthetic object on a per-object basis. Over the entire phase angle range, the median corrected diameters and albedos agree with the actual values (fractional error equals zero) within their  $1\sigma$  envelopes.

#### 4. Discussion

In Section 3 we presented the effects of individual physical and orbital properties on thermal modeling results. The largest effect is caused by the target’s solar phase angle. While this effect was already known before (see, e.g., Delbo’ 2004; Wright 2007), we quantified the magnitude of this effect in terms of the success rate and fractional errors and provided a correction function for both models. We also found that thermal modeling results of the NEATM and the FRM are barely affected by other parameters like thermal inertia, rotational period, geometric albedo, surface roughness, and pole orientation.

The parameter space explored in this work has been chosen to mimic the properties of NEAs to the best of our knowledge. While useful estimates are available for the distributions of geometric albedos and spin axis latitudes, no un-biased distributions are currently available for rotational period, thermal inertia, surface roughness, and spin axis longitude. For the other parameters, it is our intention to sample them in a wide range resembling the observed range in a uniform way. We are aware that the random combination of parameters might lead to some unrealistic configurations (e.g., a large low-albedo asteroid with a rotational period of less than a minute); we deliberately refrain from rejecting such cases in order to not distort the results of this study.

Table 1. Polynomial Coefficients of Statistical Diameter and Geometric Albedo Correction Functions.

Model	$c_0(10^{-2})$	$c_1(10^{-4})$	$c_2(10^{-6})$	$c_3(10^{-7})$
NEATM diameter	-4.7	33.4	-105.6	11.8
FRM diameter	45.3	-24.7	-95.9	5.3
NEATM albedo	6.4	-5.2	-2.1	-4.7
FRM albedo	-50.0	-19.8	148.7	-1.6

We investigate the impact of our choice of parameter ranges on the results of this work by splitting the uniform distributions in two equally sized parts at their respective median values (e.g., in the case of rotational period: short periods with  $P \leq 50$  hr and long periods with  $P > 50$  hr) and repeat the analysis discussed in Section 3 on each of these sub-samples. While these sub-sample distributions do not describe reality better than the original distribution, this approach allows us to explore the impact of an entirely different distribution on our results. We find that the results for each sub-sample agrees well with those shown in Figures 2 to 4. Differences in fractional errors are in most cases within the  $1\sigma$  envelopes – in all cases they are well-within the  $3\sigma$  envelopes. In general, FRM diameters and albedos seem to be more affected by the sub-sample parameter distributions, which is likely due to its inability to adjust its surface temperature distribution in the way the NEATM does by varying the beaming parameter  $\eta$ . In order to quantify the differences, we investigate the median fractional errors and the root-mean-square residuals between the statistical correction functions derived in Section 3.4 and the individual sub-samples over the full range in solar phase angle (0 to  $110^\circ$ ). We find median errors to be less than 5% and root-mean-square residuals to be less than 10% for all sub-samples over the full range in phase angle. Again, FRM errors tend to be higher for the aforementioned reasons. While these errors are not negligible, they are well within the typical uncertainties of thermal models (e.g., Harris et al. 2011, 20% in diameter, 50% in albedo), proving the usefulness of our approach.

Our approach in this analysis is simplistic in the sense that we only investigate effects of individual parameters, keeping the underlying distributions of all other parameters intact. However, specific combinations of the aforementioned parameters are able to significantly distort thermal modeling results. This is reflected by success rates that deviate from unity and the wide  $3\sigma$  confidence intervals of the fractional errors plotted in Figures 2 to 4. For instance, Figure 2 shows the effects of rotational period and thermal inertia on thermal modeling results separately, both of which only have a minor impact. However, it is likely that for a combination of a short rotational period and a high thermal inertia (and some other parameters) the FRM can perform better than the NEATM. Cases like these are captured by the fractional error envelopes that we derive. We deliberately do not investigate the effect of combinations of physical and orbital parameters, since this study is aimed at the thermal modeling of generic NEAs for which very little information is available. In cases in which more information is available (e.g., rotational periods, spin axis orientations, etc.) on the target body, the use of a TPM might be more appropriate and provide more accurate results.

The statistical correction functions derived in Section 3.4 have been derived from large samples of synthetic data and might not have the effect of improving the diameter estimates for individual asteroids. The corrections are meant to provide an estimate of how much the

different thermal models overestimate or underestimate diameters and albedos on average. They provide a means to correct for thermal model limitations on a statistical basis. Some of these limitations are the FRM’s inability to modulate its surface temperature distribution and the NEATM’s assumption of a lack of night side thermal emission. A different approach to the latter problem has been taken by Wolters & Green (2009) by introducing the “Night Emission Simulated Thermal Model,” which assumes a fixed surface thermal inertia that allows for an approximate determination of the thermal emission from the night side. While the NESTM has been found to provide better diameter accuracy than the NEATM for solar phase angles greater than  $45^\circ$ , it relies on a number of assumptions (fixed rotational period and thermal inertia) that may reduce its applicability to a wide range of asteroid observations. The NESTM and our statistical correction function are different approaches to the same problem, both of which may be limited in their effect on individual asteroid observations.

#### 4.1. Implications for Existing Diameter and Albedos Measurements

Diameters and albedos for about 2,500 NEAs have been derived from thermal-infrared observations. The majority of these observations have been performed during the previous decade, namely by the *Spitzer Space Telescope* (Trilling et al. 2010, 2016) and the *Wide-field Infrared Survey Explorer* (e.g., Mainzer et al. 2011b), and diameters and albedos have been derived using the NEATM. Due to spacecraft design constraints, most observations were performed near quadrature, leading to similar constraints on the solar phase angle for NEA observations from both observatories. Both the Spitzer programs (ExploreNEOs, NEOSurvey, and NEOLegacy; see the SpitzerNEOs database <http://nearearthobjects.nau.edu/spitzerneos.html>) and the WISE observations (Mainzer et al. 2011b) had a significant fraction of their targets observed at solar phase angles greater than  $65^\circ$  but generally less than  $90^\circ$ . According to Figure 4, this implies that for these observations, diameters are likely to be overestimated by up to 25% and albedos underestimated by up to 40% (relative). These effects are of the same order of magnitude as the NEATM accuracies derived by Harris et al. (2011) and hence represent a systematic effect that is not negligible.

We estimate the magnitude of this effect on the ensemble of radiometric NEA diameters and albedos available to date by querying the SpitzerNEOs database (October 2017) and find that about 25% of all Spitzer-observed NEAs were observed at solar phase angles greater than  $65^\circ$ ;  $\sim 5\%$  were observed at  $\alpha > 80^\circ$  and  $< 0.5\%$  were observed at  $\alpha > 90^\circ$ . A similar analysis for WISE-observed NEAs is not possible as observing geometries for these targets have not been published. However, according to Figure 7 in Mainzer et al. (2011b), the



ratios seem to be similar. Hence, we conclude that a small fraction ( $<5\%$ , the fraction of Spitzer-observed NEAs with  $\alpha > 80^\circ$ ) of existing NEA diameter and albedo estimates are likely to be affected by systematic effects that are of the same order of magnitude as the expected NEATM accuracy (Harris et al. 2011). We further strongly encourage researchers to include information on the observing geometry with future publications using thermal models.

## 4.2. Limitations

Our study is limited by the fact that all synthetic asteroids are assumed to be spherical and homogeneous in their properties. Furthermore, we assume no noise model in the derivation of the synthetic asteroid flux densities (flux density uncertainties following Poisson noise have been derived for the  $\chi^2$  minimization in the thermal models (Section 2.3); note that the generated fluxes have not been modified based on these uncertainties). While these simplifications allow us to better probe the effects we wanted to study, it is a gross simplification of real asteroid observations. Hence, we deliberately do not suggest that the fractional error confidence intervals shown in Figures 2 to 5 provide a measure of the accuracies that the NEATM and the FRM can provide for real asteroid observations. The result that the NEATM fractional error  $1\sigma$  confidence intervals are of the order of 10% in most cases provides merely a lower limit to the diameter accuracy that can be reached by the NEATM under idealized conditions that minimize uncertainties in the measurement process and the object’s lightcurve. In light of this lower limit, a 20% uncertainty on diameters derived with the NEATM, as derived by Harris et al. (2011), seems to be realistic. A similar argument for the albedo uncertainties is not useful, since albedo uncertainties are mainly driven by the accuracy of the target’s absolute magnitude in the optical (Harris & Lagerros 2002) and lightcurve effects.

The results of this study are also limited by the applicability of the TPM, which does not consider lateral heat conduction and is only valid in cases in which the diameter of the body is significantly larger than the thermal skin depth, which is usually of the order of a few centimeters (Spencer et al. 1989; Mueller 2007). Hence, the results of this work are valid for meter-sized and larger asteroids. However, future observations of decimeter-sized bodies in close encounters with Earth or so-called minimoons might require additional modeling for a full interpretation of the results that can be obtained from thermal-infrared observations.

### 4.3. Discussion of Individual Cases

Figures 6 and 7 illustrate two cases of synthetic asteroids observed at large and small solar phase angles, respectively, and explain the superiority of the FRM in the former and the NEATM in the latter case.

Figure 6 demonstrates why the FRM provides more accurate model diameters than the NEATM at high phase angles. The NEATM’s assumption of zero night-side emission plays an increasing role with increasing solar phase angle. At large phase angles, the NEATM assumes that a large fraction of the observed surface area is on the object’s night side and hence cold – for solar phase angles greater  $90^\circ$ , the subsolar point is not visible to the observer. For the synthetic body depicted in Figure 6, the night-side surface temperature is much higher than assumed by the NEATM. Hence, the NEATM tries to compensate for the lack of night-side emission by increasing the model diameter, yielding an overestimation of the object’s diameter. In this case, the FRM provides a better approximation of the surface temperature distribution and the object’s diameter.

Interestingly, the NEATM provides a much better fit to the object’s SED than the FRM. This is the result of the NEATM’s ability to modulate the subsolar temperature to fit the observations. However, in this case, a good fit does not equal a good approximation of the object’s diameter, since the assumptions on which the model is built describe this configuration badly. Hence, the simpler FRM provides a better approximation of this situation. The ideal solution to this problem would be to utilize a TPM to solve for the target’s diameter and albedo. However, this approach requires additional information on the target’s spin axis orientation, rotation period, and other properties. Since this wealth of information is usually not available, we suggest the comparison of NEATM and FRM results, as these will most likely bracket the real diameter and albedo.

In Figure 7, we present the surface temperature distribution of a random synthetic asteroid observed at low solar phase angles. Although the object’s surface temperature distribution is nearly iso-latitudinal, the NEATM better describes the object’s diameter, which is at least in part due to the fact that the subsolar point (the surface’s hottest point) lies within the observed hemisphere, as is assumed for the NEATM for small phase angles. Hence, low phase angle observations are usually better described with the NEATM, even though the temperature distribution is somewhat close to that of the FRM. This observation can be attributed to the fact that real asteroids have non-zero thermal inertias, finite rotational periods, and spin axis orientations that are different from the equator-on assumption on which the NEATM is built, leading to a maximum surface temperature that is lower than predicted by the subsolar temperature.

## 5. Conclusions

We investigate the effects of physical and orbital properties on the accuracy of diameters and albedos derived with the NEATM and the FRM. This analysis is done by simulating a synthetic but realistic population of NEAs and comparing the diameters and albedos derived with the NEATM and the FRM with the individual input parameters. We find the NEATM to provide more accurate diameters and albedos than the FRM in most cases, with a few exceptions. The modeling results are barely affected by the physical properties of the objects (rotational period, thermal inertia, spin axis orientation, surface roughness, and geometric albedo), but we find a large impact of the solar phase angle on the modeling results. We conclude that the NEATM provides statistically more robust diameter estimates for NEAs observed at solar phase angles less than  $\sim 65^\circ$ , while the FRM provides more robust diameters estimates for solar phase angles greater than  $\sim 65^\circ$ . This finding implies that a small percentage ( $< 5\%$ ) of all available NEA diameters (albedos) to date are overestimated by up to 25% (underestimated by up to 40%). We provide statistical correction functions for diameters and albedos derived with the NEATM and the FRM as a function of solar phase angle. The primary conclusion of this work is that errors induced by the application of the NEATM and the FRM need to be carefully modeled based on the observations in order to characterize the resulting uncertainties, especially at large phase angles.

The authors would like to thank an anonymous referee for providing useful suggestions that improved this manuscript. Some of this research was supported by NASA’s Solar System Evolution Research Virtual Institute (SSERVI) as part of the Institute for the Science of Exploration Targets (ISET) at the Southwest Research Institute (NASA grant no. NNA14AB03A). MM was supported in part by NASA grant No. NNX12AG07G from the Near Earth Object Observations program. RJ was supported in part by internal funding from the University of Hawai‘i’s Institute for Astronomy and the Office of the Vice Chancellor for Research. Computational analyses were run on Northern Arizona University’s Monsoon computing cluster, funded by Arizona’s Technology and Research Initiative Fund.

## REFERENCES

- Bolin, B., Jedicke, R., Granvik, M., Brown, P. et al. 2014, *Icarus*, 241, 280
- Delbo’, M., Harris, A. W. 2002, *M&PS*, 37, 1929
- Delbo’, M. 2004, PhD Thesis, Freie Universität Berlin

- Farnocchia, D., Chesley, S. R., Vokrouhlický, D. et al. 2013, *Icarus*, 224, 1
- Granvik, M., Vaubaillon, J., Jedicke, R. 2012, *Icarus*, 218, 262
- Harris, A. W., 1998, *Icarus*, 131, 291
- Harris, A. W., Lagerros, J. S. V. 2002, in *Asteroids III*, eds: W. F. Bottke Jr., A. Cellino, P. Paolicchi, and R. P. Binzel, University of Arizona Press, Tucson, 205
- Harris, A. W., Mommert, M., Hora, J. L., Mueller, M., Trilling, D. E. et al. 2011, *AJ*, 141, 75
- Hovis, W. A., Callahan, W. R. 1966, *J. Opt. Soc. Amer.*, 56, 639
- Lebofsky, L. A., Sykes, M. V., Tedesco, E. F. et al. 1986, *Icarus*, 68, 239
- Lebofsky, L. A. and Spencer, J. R., 1989, in *Asteroids II*, eds: Binzel, R. P., Gehrels, T., and Matthews, M. S., (Tucson: Univ. Arizona Press), 128
- Mainzer, A., Grav, T., Masiero, J., Bauer, J., Wright, E. et al. 2011, *ApJ*, 736, 100
- Mainzer, A., Grav, T., Bauer, J. et al., 2011 *ApJ*, 743, 156
- Mainzer, A., Usui, F., Trilling, D. E. 2015, *Asteroids IV*, Patrick Michel, Francesca E. DeMeo, and William F. Bottke (eds.), University of Arizona Press, Tucson, 89-106
- Masiero, J., Jedicke, R., Ďurech, J. et al., 2009, *Icarus*, 204, 145
- Mommert, M. 2013, PhD Thesis, Freie Universität Berlin, [http://www.diss.fu-berlin.de/diss/receive/FUDISS\\_thesis\\_000000095090?lang=en](http://www.diss.fu-berlin.de/diss/receive/FUDISS_thesis_000000095090?lang=en)
- Mommert, M., Hora, J. L., Farnocchia, D., Trilling, D. E., Chesley, S. R. et al. 2014, *ApJ*, 786, 148
- Mommert, M., Farnocchia, D., Hora, J. L., Chesley, S. R., Trilling, D. E. et al. 2014, *ApJL*, 789, L22
- Morrison, D. and Lebofsky, L. A. 1979, in *Asteroids*, ed: T. Gehrels (Tucson: Univ. Arizona Press), 184
- Moskovitz, N., Thirouin, A., Binzel, R. et al. 2015, IAU General Assembly, Meeting #29, id. 2255616
- Müller, T.G., Sterzik, M.F., Schütz, O. et al. 2004, *A&A*, 424, 1075

- Mueller, M. 2007, PhD Thesis, Freie Universität Berlin
- Spencer, J. R., Lebofsky, L. A., Sykes, M. V. 1989, *Icarus*, 78, 337
- Tardioli, C., Farnocchia, D., Rozitis, B. et al. 2017, *A&A*, 608, A61
- Trilling, D. E., Mueller, M., Hora, J. L. et al., 2010, *AJ*, 140, 770
- Trilling, D. E., Mommert, M., Hora, J. et al., 2016, *AJ*, 152, 172
- Usui, F., Kuroda, D., Müller, T. G. et al., 2011, *PASJ*, 63, 1117
- Warner, B. D., Harris, A. W., Pravec, P. 2009, *Icarus*, 202, 134, Updated 2016 February, <http://www.MinorPlanet.info/lightcurvedatabase.html>
- Werner, M. W., Roellig, T. L., Low, F. J., Rieke, G. H., Rieke, M. et al. 2004, *ApJS*, 154, 1
- Wolters, S. D. & Green, S. F. 2009, *MNRAS*, 400, 204
- Wright, E. L. 2007, ArXiv, astro-ph/0703085v2
- Wright, E. L., Eisenhardt, P. R. M., Mainzer, A. K. et al., 2010, *AJ*, 140, 1868
- Wright, E. L., Mainzer, A. K., Masiero, J., Grav, T., Bauer, J. 2016, *AJ*, 152, 79

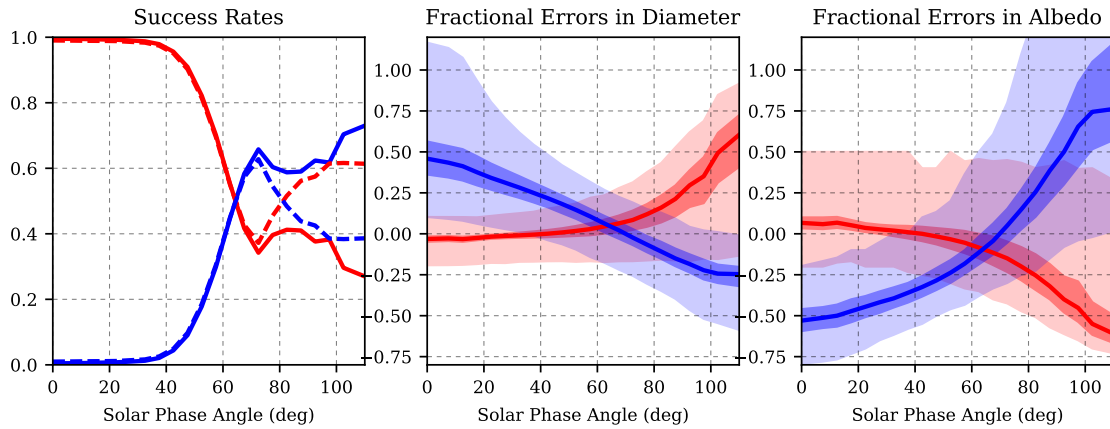


Fig. 4.— Success rates and fractional errors based on solar phase angle. Refer to Figure 2 for definitions. There is a strong dependence of the success rates and fractional errors of the NEATM and the FRM as a function of solar phase angle. FRM diameters are generally closer to the real diameters than NEATM diameters for phase angles greater  $65^\circ$

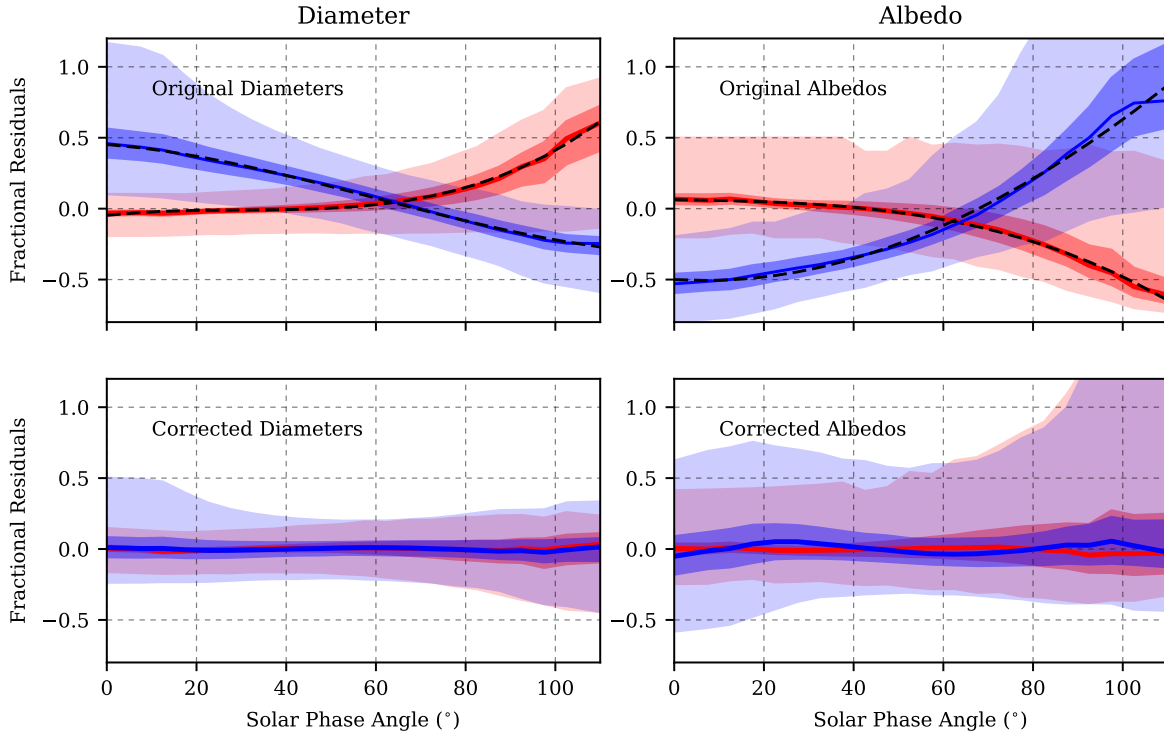


Fig. 5.— **Top:** NEATM and FRM fractional errors in diameter (left) and geometric albedo (right). The same data are shown as in Figure 4. The dashed lines are statistical offsets derived through third order polynomial fits to the median fractional errors as a function of solar phase angle. **Bottom:** The same distributions as shown in the top panel after the statistical offsets have been subtracted from the derived diameters/albedos on a per-object basis. The median fractional errors of the corrected diameters and albedo are close to zero over the entire phase angle range.

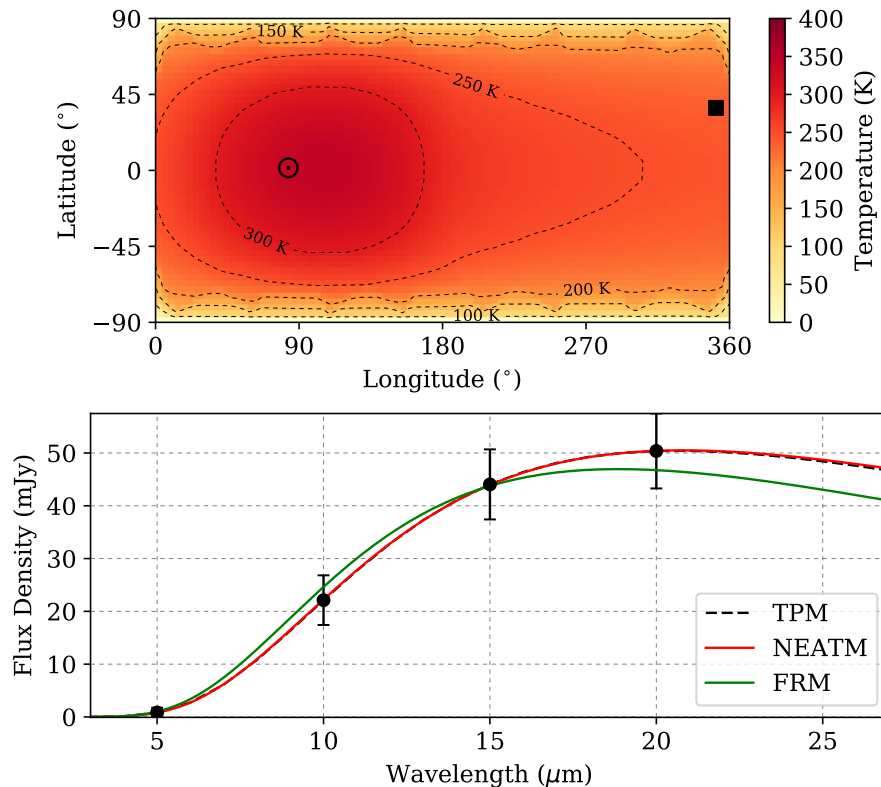


Fig. 6.— Surface temperature distribution of a random synthetic NEA observed at high solar phase angle (compare to Figure 1.) The subsolar point is indicated by a Sun symbol; the sub-observer point is indicated by a black square. For this example (rotational period of 0.55 hr, thermal inertia of 200 SI units), the FRM provides a much better diameter estimate (0.37 km instead of the real diameter 0.45 km; geometric albedo: 0.81 instead of the real geometric albedo 0.55) than the NEATM (0.78 km, geometric albedo: 0.18), although the NEATM fits the object’s SED much better than the FRM (bottom panel). This discrepancy is a result of the fact that the NEATM assumes zero thermal emission from the night-side of the object, which is clearly not the case as shown in the top panel, leading to an overestimation of the object’s diameter.



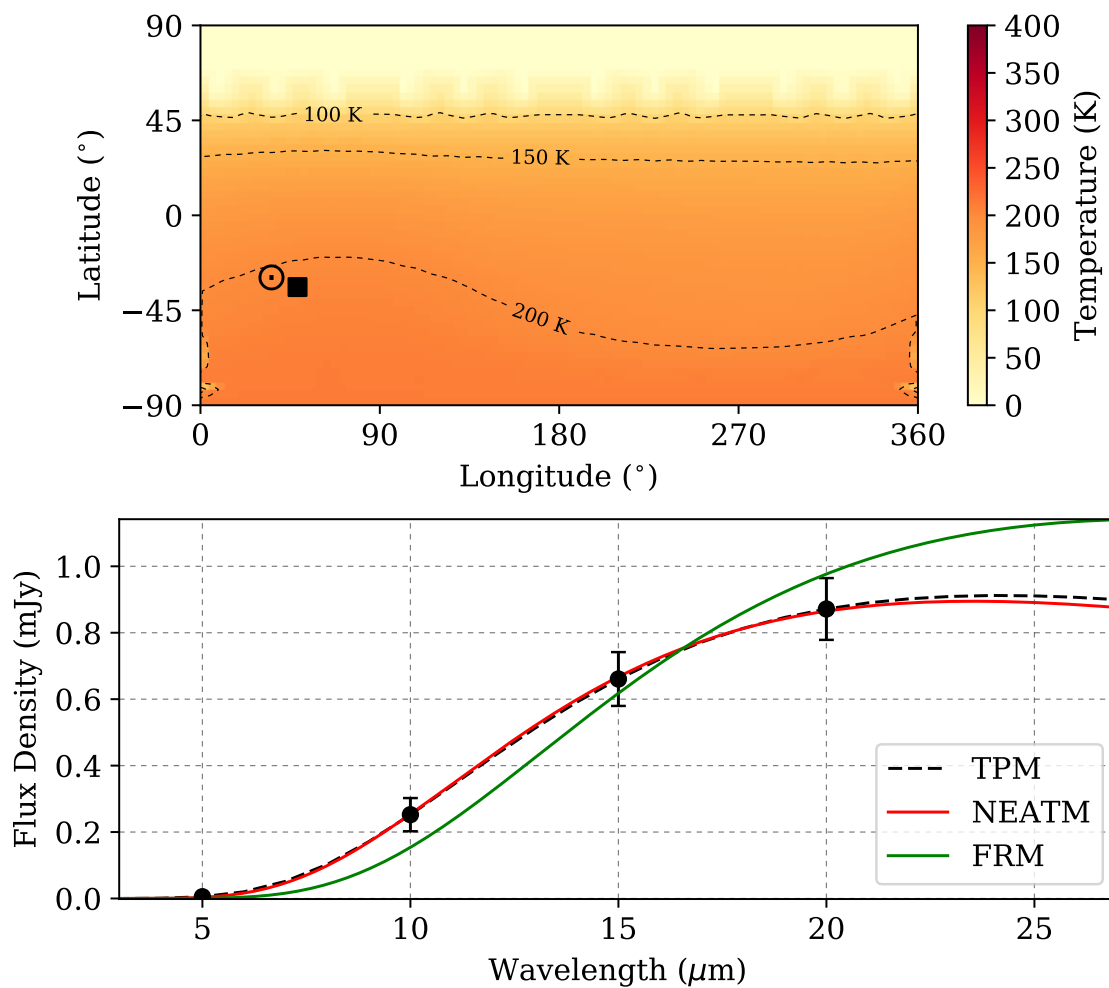


Fig. 7.— Surface temperature distribution of a random synthetic NEA observed at low solar phase angle (compare to Figure 1.) The subsolar point is indicated by a Sun symbol; the sub-observer point is indicated by a black square. For this example (rotational period of 0.28 hr, thermal inertia of 458 SI units), the NEATM provides much better results (diameter: 0.6 km, real diameter: 0.63 km; geometric albedo: 0.3, real geometric albedo: 0.28) than the FRM (diameter: 0.86 km, geometric albedo: 0.15), and it also provides the better fit to the object’s SED. Note how the NEATM provides a better estimate of the object’s diameter, even though the NEA’s surface temperature distribution is nearly iso-latitudinal.